Research Square

Preprints are preliminary reports that have not undergone peer review.
They should not be considered conclusive, used to inform clinical practice,
or referenced by the media as validated information.

Niche partitioning underpins enhanced nitrogen removal in a hybrid granular-biofilm CANON system

Jun-hao Jiang
Zhejiang Ocean University
Shi-han Zhu
Zhejiang Ocean University
Fu-hao Li
Zhejiang Ocean University
Hai-xia He
Zhejiang Ocean University
Xiao Fang
Zhejiang Ocean University
Ya-lei Liu
Zhejiang Ocean University
Li-juan Feng
Zhejiang Ocean University
Guang-feng Yang
ygfscu@126.com

Zhejiang Ocean University

Research Article

Keywords: CANON process, Biofilm, Granular sludge, Nitrogen removal performance, Microbial community, Functional gene

Posted Date: November 12th, 2026

DOI: https://doi.org/10.21203/rs.3.rs-11083265/v1

License: This work is licensed under a Creative Commons Attribution 4.0 International License.
Read Full License

Additional Declarations: No competing interests reported.

Niche partitioning underpins enhanced nitrogen removal in a hybrid granular-biofilm CANON system

Jun-hao Jiang[a], Shi-han Zhu[a], Fu-hao Li[a], Hai-xia He[a], Xiao Fang[a], Ya-lei Liu[a], Li-juan Feng[a,b], Guang-feng Yang[a,b*]

[a]Department of Environmental science and Engineering, Zhejiang Ocean University, No.1 Haida South Road, Zhoushan 316022, P.R. China

[b]Zhejiang Key Laboratory of Pollution Control for Port-Petrochemical Industry, Zhoushan 316022, P.R. China

[*]Corresponding author: Guang-feng Yang

E-mail address: ygfscu@126.com; yanggf@zjou.edu.cn.

Address: Department of Environmental science and Engineering, Zhejiang Ocean University, No.1 Haida South Road, Zhoushan 316022, P.R. China.

Abstract: This study developed a hybrid CANON reactor integrating multiple biofilm carriers with granular sludge to enhance the start-up efficiency and operational stability. The system first achieved high anammox performance under micro-aerobic conditions with total nitrogen removal efficiency (TNRE) of 89.27% ± 1.16%, and then successfully started up the CANON process through stepwise reduction of influent nitrite. Quantitative analysis revealed that carrier biofilms contributed 48.23% of the total nitrogen removal capacity, effectively complementing granular sludge activity. Microbial community analysis indicated that polyurethane carriers specifically enriched *Candidatus Jettenia* (21.02%), while large granular sludge (>2 mm) predominantly enriched *Candidatus Brocadia* (18.67%). The distribution of functional genes further confirmed a higher relative abundance of anammox-related genes (*hzs* and *hdh*) in biofilm compartments and carriers significantly enhanced sludge retention, minimizing biomass washout. The integrated system demonstrated enhanced resilience through partitioned microbial niches, providing an effective strategy for stable nitrogen removal in CANON systems.

Keywords: CANON process; Biofilm; Granular sludge; Nitrogen removal performance; Microbial community; Functional gene

Introduction

The continuous discharge of substantial amounts of domestic and industrial wastewater leads to the migration of nitrogen into water environment and the atmosphere, causing a series of environmental issues including excessive nitrogen in water bodies, eutrophication, and ecosystem imbalance (Ye et al. 2022; Derco et al. 2024; Majtacz et al. 2024). The traditional nitrification - denitrification process relies on the synergistic effects of different functional bacteria, including ammonia-oxidizing bacteria (AOB), nitrite-oxidizing bacteria (NOB), and denitrifying bacteria (DB) to remove nitrogen (Keren et al. 2020; Derco et al. 2024). However, when treating high NH_4^+-N and low C/N ratio wastewater, this process often suffers limited nitrogen removal efficiency due to the deficiency of organic carbon sources (Derco et al. 2024). Supplementing external organic carbon not only increases operational costs, but also carries the risk of secondary pollution (Kraiem et al. 2019; Derco et al. 2024), thereby seriously restricting its economical and sustainable application in practical engineering.

The completely autotrophic nitrogen removal over nitrite (CANON) process, based on the combination of partial short-cut nitrification and anammox, has become a research hotspot for nitrogen removal form wastewater due to its outstanding advantages such as no external organic carbon requirement, low operating costs, and nearly no sludge production (Luo et al. 2024; Chang et al. 2025a). In this process, AOB oxidize partial NH_4^+-N into NO_2^--N within a single reactor, after which anammox bacteria (AnAOB) directly convert the remaining NH_4^+-N and NO_2^--N into nitrogen gas (Luo et al. 2024; Xia et al. 2024; Chang et al. 2025; Xu et al. 2025). Although the CANON process has significant theoretical promise, its practical application still faces challenges such as long start-up periods and poor operational stability, mainly due to the difficulty in maintaining the balance of functional

49 microbial communities (AOB and AnAOB), as well as the system's sensitivity to sludge loss and
50 biofilm structure (Garcíaruiz et al. 2018; Yue et al. 2018; Gong et al. 2023).

51 To overcome the aforementioned limitations, recent studies have begun to explore the integration of
52 biofilm and granular sludge processes, aiming to establish composite systems that enhance microbial
53 community retention and spatial stratification (Liu et al. 2016; Gilbert et al. 2013; Chang et al. 2025a;
54 Luo et al. 2025). Biofilm can provide internal anaerobic zones suitable for AnAOB, while granular
55 sludge facilitates the formation of an external aerobic and internal anaerobic microenvironment,
56 thereby promoting synergistic interactions between AOB and AnAOB (Nielsen et al. 2005; Tsushima et
57 al. 2007; Wang and Gao 2016). Nevertheless, a systematic and in-depth investigation into the temporal
58 dynamics of microbial communities and functional genes, as well as the partitioning of nitrogen
59 transformation pathways between the biofilm and granular sludge compartments, is still needed.

60 Based on this rationale, this study was operated to test the overarching hypothesis that a hybrid
61 system integrating granular sludge with multiple biofilm carriers can enhance the performance and
62 stability of the CANON process by creating complementary microenvironments for key functional
63 microorganisms. Accordingly, a hybrid CANON reactor was established, incorporating granular sludge
64 and four distinct biofilm carriers. The reactor was operated under a three-stage strategy, i.e.
65 encompassing micro-aeration anammox, transition via nitrite reduction, and hydraulic load shocks, to
66 evaluate its operation performance. The main objectives of this study were to: 1) investigate the
67 changes in nitrogen removal and extracellular polymeric substances (EPS) characteristics, 2)
68 characterize the microbial structure and its evolution in different sludge particle sizes and carrier
69 biofilms, and 3) quantify the nitrogen transformation-related functional genes and the respective

contributions of granular sludge and biofilm to the overall nitrogen removal. Ultimately, this study provides a mechanistic understanding of microbial niche formation in hybrid systems, offering a practical strategy for optimizing the CANON process.

Materials and Methods

Synthetic wastewater

The synthetic wastewater used as influent in this study comprised $(NH_4)_2SO_4$, $CaCl_2$ (0.1 g L^{-1}), $NaHCO_3$ (1 g L^{-1}), $MgSO_4 \cdot 7H_2O$ (0.3 g L^{-1}), KH_2PO_4 (27 mg L^{-1}), and trace elements (1.25 ml L^{-1}). The trace elements were chelated with EDTA, and their main components were consistent with those reported by Chang et al. (2025a).

Experimental apparatus and operating procedures

The experimental setup used in this study was an upflow CANON reactor with the effective volume of 18 L (Fig. 1). The operation temperature of CANON reactor was 30 ± 1 ℃. It was inoculated with 5.5 L of mature anammox granular sludge and supplemented 460 polyurethane cubes (1 cm × 1 cm × 1 cm each, total packing volume of 460 mL) as biofilm carriers. The experiment is divided into three operational phases, i.e. P1 (Days 1-80), P2 (Days 81-165), and P3 (Days 166-197).

Phase 1 (days 1-80) represented the anammox operation stage under micro-aeration conditions. During this phase, the hydraulic retention time (HRT) and dissolved oxygen (DO) concentration were 14.4 h and 0.28 ± 0.11 mg L^{-1}, respectively. In Phase 2 (days 81-165), the CANON biofilm process was established by gradually reducing the NO_2^--N level, with a controlled DO of 0.68 ± 0.18 mg L^{-1}. The influent NO_2^--N was halved every 10 days and was completely eliminated starting on day 112. To mitigate free ammonia (FA) inhibition, the influent NH_4^+-N was decreased from 98.0 to 58 mg L^{-1} on

Day 116. Beginning on Day 134, the influent NH_4^+-N level was gradually increased back to 98 mg L^{-1} over a 10-day period.

On Day 154, an additional 1.6 L of mature anammox sludge was introduced into the CANON reactor, along with various biofilm carriers, including porous cylindrical carriers (100 units, total volume 200 mL), spherical packing carriers (8 units, total volume 40 mL), and elastic filler carriers (3 units, with total length of 174 cm). Following the stable establishment of the CANON biofilm process, the operational performance and stability were assessed by altering the hydraulic loading during the P3 stage (Days 166-197), under an average DO level of 0.90 ± 0.14 mg L^{-1}. The HRT was progressively reduced from 14.4 h to 10.78 h (Days 165-173), 8.65 h (Days 174-180), and 7.2 h (Days 180-186), and then being restored to the initial value of 14.4 h. The key operational parameters of CANON reactor at each operation phase are summarized in Table 1.

Analysis of CANON activity and contribution of carrier biofilm to nitrogen removal

At the end of the experiment, the contribution of sludge and biofilm to nitrogen removal within the CANON system was evaluated. The sludge and all carrier biofilms were removed from the main reactor and transferred into two parallel reactors (R1 and R2), which were operated continuously for 8 days under identical influent NH_4^+-N level of 50 mg L^{-1}. Daily water samples were collected for analysis of NO_2^--N, NO_3^--N and NH_4^+-N levels. Simultaneously, the sludge loss of of both reactors was collected each day, and its volume was recorded to determine the sludge volume index after 30 minutes (SV_{30}), suspended solids (SS), and volatile suspended solids (VSS). The specific anammox activity (SAA) was then obtained by dividing the removal rates of NH_4^+-N, NO_2^--N, and total nitrogen (TN) by the VSS concentration.

Analytical methods for water quality indicators

Water quality indicators, including NO_3^--N, NH_4^+-N, NO_2^--N, and pH, were regularly monitored in both influent and effluent of CANON reactor. The NO_3^--N, NH_4^+-N and NO_2^--N were determined using ultraviolet spectrophotometry, phenol hypochlorite spectrophotometry and N - (1-naphthyl) - ethylenediamine spectrophotometry, respectively. A portable pH meter (Mettler Toledo, Shanghai) was employed for pH measurements.

Analysis of EPS and 3D-EEM spectroscopy

At the end of this experiment, different EPS fractions of CANON sludge was analyzed by quantifying the primary components of protein (PN) and polysaccharide (PS) contents, including soluble EPS (S-EPS), loosely bound EPS (LB-EPS), and tightly bound EPS (TB-EPS), following the analytical procedure described by Zhang et al. (2024). PN and PS were determined using the improved Lowry Folin method (Frøelund et al. 1995) and the anthrone–sulfuric acid method (Loews et al. 1952), respectively. The 3D-EEM spectroscopy was performed in accordance with the methodology outlined by Chang et al. (2025b).

Analysis of microbial structure and functional genes

At the end of this experiment, sludge and various biofilm samples were obtained for microbial community structure sequencing on a Illumina HiSeq 2500 platform. Genomic DNA was extracted from the samples using the OMEGA E.Z.N.A.® Mag-Bind Soil DNA Kit. After quantification with Qubit 2.0, PCR amplification was carried out in a 30 μL reaction system. Each reaction contained 15 μL of 2× Master Mix, 1 μL each of bar-coded forward (Primer F) and reverse (Primer R) primers, 10-20 ng of template DNA, and ultrapure water to adjust the final volume to 30 μL. Amplification

products were purified and recovered based on type and fragment size: bacterial, archaeal, and other fragments ≥ 400 bp were treated with 0.6× magnetic beads, whereas fungal and other fragments < 400 bp were processed with 0.8× magnetic beads. After binding, washing, and elution steps, the purified DNA was re-quantified using Qubit 2.0. Equimolar amounts (10 ng) of each sample were pooled to achieve a final loading concentration of 20 pmol.

The raw sequencing data were evaluated by FastQC and filtered using Trimomatic. Valid sequences were assembled with IDBA-UD, and optimal contigs were selected through comprehensive evaluation. Following assembly, open reading frames (ORFs) were predicted from the contigs using Prodigal. Predicted genes ≥ 100 bp in length were retained and translated into amino acid sequences. These sequences were subsequently deduplicated using CD-HIT to generate a non-redundant gene catalog. Finally, Bowtie2 was used to align each sample sequence to the gene set, and the gene abundances in each sample were obtained using SAMtools.

Results and Discussion

Performance of anammox system under micro-aeration conditions (stage P1)

The operational performance of reactor at each stage is shown in Fig. 2. The removal efficiencies of NH_4^+-N, NO_2^--N, and TN were 96.26% ± 0.66%, 99.67% ± 0.20%, and 89.27% ± 1.16%, respectively. The corresponding TN loading rate (TNLR) and TN removal rate (TNRR) of the reactor were 0.36 ± 0.01 and 0.32 ± 0.01 kg m^{-3} d^{-1}, respectively. Under a micro-aeration conditions (DO = 0.28 ± 0.11 mg L^{-1}), the system showed good nitrogen removal performance and maintained stable operation throughout the 80-day operation in P1, primarily attributed to the DO gradient formed under micro-aerobic conditions. This gradient facilitated the enrichment of AOB in the outer layer of the

154 granular sludge and biofilm, oxidizing part of NH_4^+-N to NO_2^--N, while the inner anoxic zone provided
155 an ideal habitat for AnAOB to perform anammox reaction (Chang et al. 2025a; Luo et al. 2024; Yu et al.
156 2021). Furthermore, the stable operational performance indicates that inoculating mature anammox
157 granular sludge combined with micro-aerobic regulation can effectively promote the functional synergy
158 between AOB and AnAOB while avoiding the inhibition of AnAOB by high DO (Fu et al. 2025; Xu et
159 al. 2025).

160 *Operational characteristics during the transition to the CANON process via gradual substrate*
161 *reduction (stage P2)*

162 At the beginning of stage P2, the influent NH_4^+-N concentration was 98 mg L^{-1} with NO_2^--N of 49
163 mg L^{-1}. After 10 days of operation, the effluent NH_4^+-N levels showed a decrease from 28.7 to 18.7 mg
164 L^{-1}, while the effluent NO_2^--N concentration decreased from 9.6 to 2.8 mg L^{-1}, resulting in a TNRE of
165 74.46%. Without changing the influent NH_4^+-N levels, the influent NO_2^--N levels furthter decreased to
166 24.5 mg L^{-1}. Over the subsequent 10 days, the effluent NH_4^+-N concentration decreased from 33.08 to
167 18.5 mg L^{-1}. Throughout this period, the NO_2^--N in effluent remained consistently low levels of 3.6 ±
168 0.83 mg L^{-1}, with TNRE of 69.93%.

169 Further decreasing influent NO_2^--N to 11.8 mg L^{-1}, the effluent NH_4^+-N remained elevated at 37.9
170 mg L^{-1} without evident decreasing trend, and the effluent NO_2^--N showed an increase to 14.6 mg L^{-1},
171 resulting in a decline in nitrogen removal performance. By day 112, without adding any NO_2^--N to the
172 influent, the effluent NH_4^+-N reached 47.6 mg L^{-1}. These results demonstrated that a gradual reduction
173 of influent NO_2^--N facilitates system adaptation and transition toward the CANON process. However,

174 complete elimination of NO_2^--N from the influent leads to significant decline in nitrogen removal
175 performance.

176 On day 115, the influent NH_4^+-N decreased to 58 mg L^{-1}. Over the following 10 days, the effluent
177 NH_4^+-N decreased from 46.8 to 22.8 mg L^{-1}, while the TNRE increased from 10.75% to 41.82%,
178 corresponding to an average daily increase of 20.2%.. These results indicated that reducing influent
179 substrate enhanced the nitrogen removal in CANON system. Furthermore, the nitrogen removal
180 performance improved markedly when DO increased from 0.28 ± 0.11 to 0.4-0.5 mg L^{-1},. Within one
181 day, the effluent NH_4^+-N concentration decreased to 7.28 mg L^{-1}, and the TNRE increased by 20.3%,
182 reaching 62.12%. After 7 days, the TNRE table at 58.96% ± 1.99%.

183 Over the subsequent 10 days, the influent NH_4^+-N increased gradually from 58.0 to 98 mg L^{-1}, with a
184 corresponding increase in DO levels to a range of 0.8 - 0.9 mg L^{-1}. Between days 144-154, the average
185 TNRE was 55.58% ± 2.37% with effluent NH_4^+-N and NO_2^--N levels of 17.7 ± 3.12 and 4.95 ± 1.15
186 mg L^{-1}, respectively. Obviously, CANON has a robust operational performance. On day 154, four
187 distinct types of biofilm carriers (polyurethane, porous cylinder, spherical packing, and elastic packing)
188 along with 1.6L of anammox sludge (VSS: 6.74g) were added into the reactor. Following a two-day
189 recovery period, the operation performance was further improved. During days 157-164d, the average
190 TNRE was 66.21% ± 4.71%, while effluent NH_4^+-N and NO_2^--N levels decreased to 13.02 ± 4.09 and
191 3.09 ± 0.83 mg L^{-1}, respectively.

192 *Stability and recovery capacity of CANON System under different hydraulic loading conditions (Stage*
193 *P3)*

During the stage P3, the HRT was reduced from 14.4 to 10.78 h on Day 165, which led to an effluent NH_4^+-N concentration of 36.0 mg L^{-1}. After 2 days' operation, the effluent NH_4^+-N decreased to 14.05 mg L^{-1}. The average effluent NH_4^+-N levels were 13.1 ± 2.3 mg L^{-1} (Days 168 - 174) with TNRE of 60.87 ±%. The average TNNR and TNLR were 0.15 ± 0.02 and 0.26 ± 0.02 kg m^{-3} d^{-1}, respectively. On day 174,TNRE was reduced to 52.98% at a decreased HRT of 8.65 h, but increased to 59.32% after four days of operation with effluent NH_4^+-N concentration decreased to 8.98 mg L^{-1}. The corresponding TNRR and TNLR values were 0.18 and 0.31 kg m^{-3} d^{-1}, respectively. When HRT was further shortened to 7.2 h on Day 180, TNRE declined from 60.06% (Day 182) to 45.48% (Day 186), indicating a pronounced suppression of nitrogen removal performance. The average TNRR and TNLR between Days 180 and 186 were 0.20 ± 0.02 and 0.36 ± 0.02 kg m^{-3} d^{-1}, respectively. After the HRT was restored to 14.4 h, the operation performance recovered within 7 days. From days 194 to 197, the average effluent NH_4^+-N level was 18.53 ± 3.00 mg L^{-1}, and the TNRE stabilized at 60.95% ± 1.73%.

The CANON system was started up through stepwise reduction of NO_2^--N in this study, adjustment of influent NH_4^+-N concentration, and controlled adjustment of DO. These results demonstrated that a gradual decrease in NO_2^--N concentration facilitates the transition to the CANON process. However, system performance became unstable when NO_2^--N was nearly completely eliminated, preventing full and successful establishment of the process. Decreasing influent NH_4^+-N levels could not improve CANON performance. Ultimately, only through precise regulation of the DO concentration could the CANON system achieve improved and stable nitrogen removal performance.

Contribution of biofilm and granular sludge to nitrogen removal and sludge retention effects

214 Following the separation of sludge and carrier biofilm into two parallel reactors (R1 and R2), their
215 8-day operational performance is shown in Fig. 3. On days 1 and 2, the TNREs in R1 were 27.94% and
216 41.62%, respectively, while those in the biofilm reactor R2 were 21.46% and 20.36%, respectively.
217 During the first four days, the average TNREs were 39.14% ± 7.73% for R1 and 18.59% ± 4.50% for
218 R2. When influent NH_4^+-N increased to 98 mg L^{-1}, TNRE in R1 remained relatively stable, averaging
219 38.38% ± 3.78%. In contrast, the TNRE in R2 increased significantly, reaching an average of 36.09% ±
220 6.85%. These results demonstrate that the carrier biofilm contributes substantially to nitrogen removal,
221 accounting for 48.23% of the total nitrogen removal capacity of CANON reactor. This result indicated
222 that the nitrogen removal of carrier biofilm is comparable to that of granular sludge.
223 The initially lower performance of R2 (biofilm reactor) can be attributed to a short-term stress
224 response induced by system separation, whereas the subsequent performance recovery highlights the
225 inherent advantages of the biofilm system, i.e. structural stability and functional resilience after
226 acclimation to the new conditions. This resilience stems from the stable microenvironment within the
227 biofilm, which favors the retention and spatial stratification of functional microbial communities,
228 enabling AOB and AnAOB to metabolize efficiently in their respective niches (Wang et al. 2022; Yu et
229 al. 2021). This phenomenon clearly demonstrates that in the integrated hybrid system, the biofilm
230 serves not only as a “habitat” for functional microorganisms but also as a core component with high
231 functional elasticity, capable of maintaining efficient nitrogen removal under dynamic operational
232 conditions.
233 In addition, the incorporated carrier biofilm also contributed to sludge retention in the system.
234 Almost no sludge washout was observed in the effluent of the integrated CANON biofilm - granular

235 sludge system. In contrast, due to the absence of carrier biofilm for sludge retention, significant sludge
236 loss occurred in reactor R1 as a result of aeration and hydraulic scouring, as summarized in Table 2.
237 The most severe sludge loss was recorded on the first day, with 21.3 g of SS and 8.3 g of VSS being
238 washed out. Thereafter, the amount of sludge loss gradually decreased, and no further loss was detected
239 from day 7 to day 8. Over the 8-day operational period, reactor R1 accumulated a total sludge loss of
240 53.4 g SS with 23.0 g VSS. This result confirmed the importance of carriers in enhancing system
241 stability (Yue et al. 2018). Studies showed that adding suitable carriers (e.g. polyurethane) can act as a
242 physical barrier, effectively immobilize AnAOB, increase biomass retention, and enhance the system's
243 resistance to loading shocks (Ahmad et al. 2020; Lv et al. 2019).

244 *Distribution and characteristics Analysis of EPS*

245 Extraction via mechanical grinding of the carrier biofilms yielded EPS contents below the detection
246 limit, and consequently no S-EPS, LB-EPS, or TB-EPS were observed. Neither S-EPS nor LB-EPS
247 were detected in the sludge extracts from any particle size fraction following high-speed centrifugation.
248 The PN and PS contents of TB-EPS are shown in Fig. 4. Sludge with larger particle sizes (>2 mm)
249 secreted EPS with higher PN and PS contents, reaching the maximum values of 120.1 and 29.1 mg L^{-1},
250 respectively. As particle size decreased, PN content declined to 95.3 (1-2 mm), 60.7 (0.5-1 mm), and
251 13.3 mg L^{-1} (0.25-0.5 mm), while corresponding PS levels decreased to 17.3, 9.0 , and 1.1 mg L^{-1},
252 respectively.

253 The PN/PS value is widely employed as an indicator of sludge particle strength and settleability, and
254 a lower value generally associated with better settling performance (Wang et al. 2020; Tang et al. 2011).
255 In this study, the PN/PS ratios for sludge of size classes >2 mm, 1-2 mm, 0.5-1 mm, 0.25-0.5 mm, and

<0.25 mm were 4.1, 5.5, 6.7, 12.4, and 12.0, respectively. These results indicated that larger sludge particles exhibited improved sedimentation characteristics. The generally high PN/PS ratios suggest favorable settling properties throughout the sludge samples. These findings align with previous studies , which also reported EPS rich in protein and elevated PN/PS ratios in the range of 2.44-12.1 (Lotti et al. 2019; Feng et al. 2019; Chen et al. 2021; Chang et al. 2025a).

This absence of measurable EPS from biofilms, despite their demonstrated substantial contribution to nitrogen removal (~48.23%) (section *Contribution of biofilm and granular sludge to nitrogen removal and sludge retention effects*), challenges conventional views and offers novel insights into the divergent life strategies within the hybrid system. This discrepancy suggests that the microbial consortia on carriers and in granules may employ fundamentally different strategies for aggregation and environmental interaction. Granular sludge, as free-floating aggregates, invests heavily in secreting copious, TB-EPS (predominantly PN) to build a self-sustained, diffusion-limited architecture (Sheng et al. 2010; Aqeel et al. 2023). This EPS matrix is crucial for creating the oxygen gradient, maintaining structural integrity, and ensuring settleability. In contrast, biofilm communities on fixed carriers may rely primarily on direct cell-surface adhesion and close cell-cell interactions within the confines of the carrier's porous structure. Their social glue might be more reliant on specific adhesins, pili, or scarce but highly effective extracellular polymers that are not extractable by standard mechanical/chemical methods (Aqeel et al. 2023; Schneier et al. 2024; Sura et al. 2025). This represents a low-investment, carrier-dependent immobilization strategy, where the physical scaffold provided by the carrier substitutes for the need to build a massive extracellular matrix from scratch.

3D-EEM spectroscopy analysis

As shown in Fig. 5, three-dimensional excitation–emission matrix (3D-EEM) analysis revealed no distinct characteristic peaks in the S-EPS and LB-EPS fractions of either sludge or biofilm samples. In contrast, three characteristic peaks were identified in the TB-EPS of sludge across all particle size fractions, with excitation (Ex)/emission (Em) wavelength of 200-250/280-330 (tyrosine-like proteins), 200-250/230-380 (tryptophan-like proteins), and 250-400/280-380 (soluble microbial byproducts), respectively. These EPS-related peaks were predominantly protein-like in nature, with the >2 mm particle size sludge exhibiting the highest protein content. This distribution of protein-like components in TB-EPS aligns with the chemical extraction results (Section *Distribution and characteristics Analysis of EPS*), further confirming that larger granules accumulate more extracellular proteins. The prevalence of these recalcitrant protein-like substances suggests their potential role in enhancing structural integrity and facilitating the formation of stable microbial aggregates, which is consistent with the excellent settling performance in the larger sludge fractions.

Analysis of microbial community structure

Diversity analysis

The diversity index for both biofilm and sludge samples are shown in Table 3. Biofilm of columnar carrier (BFCC) and spherical carrier (BFBC) exhibited higher Shannon indices and lower Simpson indices compared to bioflim on elastic filler carriers (BFESM), indicating greater microbial diversity in these two carrier types. For the biofilm on polyurethane carrier (BFPU), the Shannon index progressively increased with Simpson index decreasing from stage I to stage III, suggesting more uniform species distribution and enhanced diversity as the system transitioned from the anammox to the CANON process. Furthermore, the polyurethane carrier demonstrated higher species richness

298 relative to the other biofilm carriers. In the sludge samples, the Shannon indices remained relatively
299 stable across the three operational stages, with values of 12.53, 12.82, and 12.50, respectively. Among
300 different sludge particle sizes, both the >2 mm and <0.25 mm fractions showed similarly high Shannon
301 indices, reflecting elevated microbial diversity. In contrast, the 0.25-0.5 mm particle size sludge
302 displayed the lowest diversity, as indicated by a Shannon index of 11.60.

303 Microbial community structure at phylum level

304 There were 12 phyla exhibited a relative abundance (RA) greater than 1% in granular sludge and
305 biofilm samples (Fig. 6a). During stage P1, the microbial community was co-dominated by
306 Proteobacteria (27.01%) and Planctomycetes (21.12%), which showed comparable RA values. During
307 stage P2, Proteobacteria (26.58%) and Planctomycetes (16.65%) remained the predominant phyla,
308 though their RA values slightly decreased compared to P1. In stage P3, the RA of Proteobacteria
309 increased to 34.28%, making it the absolutely dominant phylum, while the RA of Planctomycetes
310 decreased to 8.48%. This result may be associated with the more favorable conditions for AOB growth
311 under higher DO (Luo et al. 2024).

312 AnAOB primarily belong to the phylum Planctomycetes (Wang et al. 2014), and their abundance can
313 reflect whether the anammox process is being inhibited to some extent (Zhou et al. 2021). In contrast,
314 AOB are mainly affiliated with the phylum Proteobacteria (Wang et al. 2019). The shifting RA values
315 of Proteobacteria and Planctomycetes across the three stages in this study suggest a potential transition
316 in the dominant nitrogen transformation pathway. Chloroflexi was also identified as a dominant
317 phylum, with relatively stable RA values of 8.27%, 8.04%, and 8.38% in stages I, II and III,
318 respectively. In biological wastewater treatment research, certain reported Chloroflexi bacteria with

facultative anaerobic characteristics can decompose and utilize macromolecules released by dead cells and serve as structural scaffolds in sludge, thereby playing an important symbiotic role in maintaining the granular stability and enhancing their adaptability to environmental changes (Gong et al. 2020; Hu et al. 2023).

The RA of dominant phyla also varied with sludge particle size. Proteobacteria was the predominant phylum in the 0.25-0.5 mm and <0.25 mm sludge fractions, with RAs of 27.16% and 27.42%, respectively. In the 0.5-1 mm fraction, Proteobacteria remained dominant at 26.15%, substantially higher than the RA of Planctomycetes (15.42%). In contrast, both Planctomycetes and Proteobacteria were dominant in the 1-2 mm and >2 mm sludge, though Planctomycetes exhibited higher RA values of 30.85% and 38.86%, respectively.

The BFPU participated in the CANON process throughout all three operational stages, and its microbial community dynamics closely similarly to those of the system sludge across these stages. In the BFPU biofilm, Proteobacteria and Planctomycetes were the dominant phyla. During stage P1, their RA were 22.50% and 31.20%, respectively. By stage P3, the RA of Proteobacteria increased to 30.79%, establishing it as the absolutely dominant phylum in the system. Similarly, Proteobacteria, Planctomycetes, and Chloroflexi were the dominant phyla in BFBC, BFCC, and BFESM biofilm. Among these, Proteobacteria constituted the overwhelming majority, with RAs of 29.11%, 26.58%, and 38.82%, respectively. Notably, the RA of Proteobacteria in the BFESM carrier was substantially higher than in all other carriers tested.

Microbial community structure at genus level

339 Fig. 6b shows the microbial community structure at the genus level across the three operational
340 stages and for each sludge particle size fraction. The primary AnAOB genera identified in the CANON
341 system were *Candidatus Jettenia* and *Candidatus Brocadia*, in line with their well-established roles in
342 such processes (Wang et al. 2019). Meanwhile, the key AOB genus *Nitrosomonas* (Zhu et al. 2022;
343 Chang et al. 2025a) and the dominant NOB genus *Nitrospira* were also detected.

344 In stage P1 with DO levles of 0.28 ± 0.11 mg L^{-1}, anammox reaction was dominant in the reactor,
345 with dominant AnAOB genera *Candidatus Jettenia* (10.32%) and *Candidatus Brocadia* (7.09%). At the
346 same time, the AOB genus *Nitrosomonas* and NOB genus *Nitrospira* had RA values of 0.31% and
347 0.56%, respectively. In stage P2, the RA value of *Candidatus Jettenia* decreased to 3.54%, while the
348 RA value of *Candidatus Brocadia* increased to 8.93%. Due to the increase in DO, the RA values of
349 *Nitrosomonas* and *Nitrospira* increased to 2.00% and 1.38%, respectively. In stage P3, the RA values of
350 *Candidatus Jettenia* and *Candidatus Brocadia* further declined to 1.75% and 3.37%, respectively. At
351 the same time, the RA values of *Nitrosomonas* and *Nitrospira* remained relatively stable at 2.02% and
352 1.37%, respectively.

353 The RA of microbial communities varies with sludge particle size. For sludge with particle sizes of
354 1-2mm and>2mm, the RAs of AnAOB genera *Candidatus Jettenia* (7.07% and 16.65%) and
355 *Candidatus Brocadia* (18.67% and 18.63%) were much higher than those in other size fractions. The
356 RAs of *Candidatus Jettenia* and *Candidatus Brocadia* in sludge with a particle size<1mm were 6.55%
357 and 14.72%, respectively.

358 AOB *Nitrosomonas* and NOB *Nitrospira* were mainly distributed in sludge with smaller particle
359 sizes. In the 0.5-1 mm fraction, the RA values of *Nitrosomonas* and *Nitrospira* were 1.70% and 1.18%,

respectively. These values increased to 2.14% and 2.50% in the 0.25-0.5 mm fraction, and further to 2.35% and 2.09% in the <0.25 mm fraction. In sludge with particle sizes >1 mm, the RA values of *Nitrosomonas* and *Nitrospira* were considerably lower at 1.36% and 0.95%, respectively. The structure of large sludge particles facilitates the formation of a dual-layer configuration, comprising an inner anaerobic zone and an outer aerobic zone. This structure promotes the enrichment of AnAOB in the interior, while AOB and NOB dominate the exterior. In contrast, DO readily penetrates small sludge particles, resulting in a larger aerobic volume fraction, which supports the enrichment of AOB and NOB at higher abundances.

The PU carrier was present from Day 1, accompanying the system through the entire evolutionary journey (P1-P3). As shown in Fig. 6c, the RA of AnAOB in BFPU biofilm gradually decreased over the operational period, whereas the RA of nitrifying bacteria increased. During stages P1, P2, and P3, the RA values of AnAOB genus *Candidatus Jettenia* were 21.02%, 2.76%, and 1.34%, respectively, while the RA values of *Candidatus Brocadia* were 7.12%, 6.82%, and 3.86%, respectively. The corresponding RA values of AOB genus *Nitrosomonas* were 0.24%, 1.45%, and 1.38%, respectively. At the same time, the RA values of NOB genus *Nitrospira* were 0.61%, 2.17%, and 4.24%, respectively. This suggests the BFPU developed integrated micro-niches supporting both partial nitrification and anammox, making it a functionally versatile and stable compartment.

In stark contrast, the CC, BC, and ESM carriers were introduced on Day 154, directly into a system where CANON metabolism was already active under a higher DO (P3). Their biofilms formed under a strong and immediate selective pressure favoring microorganisms adapted to the prevailing conditions. The results show a clear divergence among these latecomers, likely dictated by their intrinsic physical

properties. The RA values of AnAOB genus in BFESM biofilm were higher than those in BFBC and BFCC biofilm. Specifically, the RAs of *Candidatus Jettenia* and *Candidatus Brocadia* in BFESM were 2.42% and 4.72%, respectively. These values were higher than those in BFBC (0.82% and 2.41%) and BFCC (0.67% and 1.73%). The RA values of AOB and NOB in carrier BFBC were higher than those in BFCC and BFESM. The highest RAs of *Nitrosomonas* (2.53%) and *Nitrospira* (8.77%) were found in BFBC, exceeding their levels in BFCC (1.12% and 4.32%), BFESM (0.97% and 0.86%), and BFPU (1.38% and 4.24%). These results indicated that BFPU and BFESM facilitate the formation of anaerobic zones and support the enrichment of AnAOB, whereas BFBC favors the growth of AOB and NOB, suggesting that nitrification is the dominant process in its biofilm.

The carrier function observed in P3 is a product of both inherent physical properties and historical contingency (i.e., the conditions during initial biofilm formation) (Fukami 2015). BFESM exemplifies a carrier that successfully developed and retained an anammox biofilm through a gradual environmental shift, a process that benefits from prolonged acclimation. BFBC/BFCC represent carriers whose biofilm assembly was primed towards nitrification due to their late introduction into a nitrifying environment. This insight has significant practical implications: it suggests that the timing of carrier addition could be used as a control parameter to guide biofilm functionality in hybrid systems. To cultivate anammox-dominated biofilms, carriers should be introduced early under conducive (low-DO) conditions. If aiming to enhance nitrification capacity, adding specific carriers later during the nitrification phase might be an effective strategy.

Functional gene analysis

The composition of functional genes related to nitrogen removal in each sludge sample is shown in Fig. 7a. The experimental results showed that functional genes associated with partial nitrification, specifically ammonia monooxygenase (*amo*) and hydroxylamine oxidoreductase (*hao*) gene, exhibited the highest RAs in sludge samples. The RA values of *amo* gene in P1, P2, and P3 were 0.2%, 0.18%, and 0.15%, respectively. The corresponding RA values of *hao* gene were 0.07%, 0.05%, and 0.02%, respectively. In terms of particle size, the RA of the *amo* gene was 0.27% ± 0.01% and 0.11% ± 0.02% in sludge with particle sizes >1 mm and ≤1 mm, respectively. Corresponding values for *hao* gene were 0.18% ± 0.03% and 0.05% ± 0.03%, respectively. These findings collectively highlight the critical role of partial nitrification genes across different operational phases and sludge particle sizes, with larger particles (>1 mm) maintaining higher functional gene abundance.

Genes encoding key enzymes specific to anammox, including hydrazine synthase (*hzs*) and hydrazine dehydrogenase (*hdh*) exhibited high RA. Additionally, high RA values were observed for genes encoding various nitrite reductases (*NIR*), including the dissimilatory enzymes *nirS* and *nirK* (primarily associated with denitrification) and the assimilatory enzyme *nirB*. Throughout the three operational stages of the CANON system, the RA of anammox-specific functional genes remained stable. However, the abundances of *hdh*, *hzs*, and *NIR* genes were consistently higher in sludge with particle sizes >1 mm compared to smaller particle size fractions, confirming at the molecular level the promotive effect of the anoxic microenvironment within large granules on AnAOB metabolic activity (Chang et al. 2025b; Zhang et al. 2024) and potential denitrification processes (Zhang et al. 2020).

Functional genes associated with nitrification were identified, including those encoding nitrite oxidoreductase (*nxrA/B*), assimilatory nitrate reductase (*nirA*, *nasA*), and the membrane-bound nitrate

reductase (*narG*). Throughout the three operational stages, nitrification activity increased with rising DO concentration. The RA of the *nxrB* gene remained stable, whereas that of *nxrA* increased from 0.059% in stage P1 to 0.092% in stage P3. These nitrification-related functional genes were detected across all sludge particle sizes, with no significant differences in RA among size fractions. Genes related to nitrate assimilation (*nirA*, *nasA*) were also detected. Their RA showed no notable variations across different operational stages or sludge particle size fractions, consistent with the observation that assimilatory nitrate reduction was not a dominant nitrogen transformation pathway in this system.

The distribution of functional genes across the four carrier biofilms is shown in Fig. 7b. The RA of anammox- and nitrification-associated genes in the BFPU carrier biofilm declined, mirroring the trend observed in the sludge. Specifically, the RA of the *amo* gene decreased from 0.26% in stage P1 to 0.18% in P2 and 0.16% in P3, while the RA of the *hao* gene declined from 0.11% to 0.04% and 0.02% across the same stages. Furthermore, the RA of anammox-related functional genes was higher in the BFESM biofilm than in the BFCC and BFBC biofilms, reaching a level comparable to that in the BFPU biofilm.

The RA of functional genes associated with nitrification was similarly high in the BFCC and BFBC biofilms compared to other carriers. In contrast, the RA of genes of nitrate assimilation (*nirA* and *nasA*) showed no significant changes across different carriers or operational stages in the BFPU biofilm. Additionally, the *hox* gene was detected in the reactor, with its RA remaining stable at approximately 0.05%-0.06% in all biofilm and sludge samples. This finding is consistent with the study reported by Marcel et al. (2018), which identified the *hao* gene, encoding hydroxylamine oxidoreductase, as a

functional component in anammox systems, where it may recover hydroxylamine leaked from hydrazine synthase (HZS).

Consistent with the microbial community analysis, the functional gene profiles in Stage P3 solidify the carrier-specific roles. The high RA of anammox-related genes (*hzs*, *hdh*) in ESM biofilm and their decline in PU biofilm from P1 to P3 likely reflect a functional adaptation where PU biofilm, despite retaining high AnAOB cell counts, might have downregulated or diversified its anammox gene complement under elevated DO. Conversely, the sustained high RA of nitrification genes (amo, nxr) in BC and CC biofilms confirms their active role as nitrification hotspots in the operational CANON system. This genetic evidence underscores that the choice of carrier material not only selects for microbial populations but may also influence their metabolic state and functional gene expression under process-relevant conditions.

Conclusions

This study successfully developed and validated a hybrid CANON system integrating multiple biofilm carriers with granular sludge, demonstrating significant improvements in start-up efficiency, operational stability, and resilience to disturbances. The system achieved high anammox performance under micro-aerobic conditions and was successfully transitioned to stable CANON operation through stepwise reduction of influent nitrite. Biofilm carriers contributed approximately 48.23% of the total nitrogen removal capacity, functionally complementing the granular sludge. Microbial analysis revealed spatial partitioning of functional communities between carriers and sludge: PU carriers specifically enriched *Candidatus Jettenia* (21.02%), while large granular sludge (>2 mm) predominantly enriched *Candidatus Brocadia* (18.67%). Higher RAs of anammox-related functional

463 genes (*hzs*, *hdh*) were detected in biofilm compartments. Furthermore, carriers enhanced sludge
464 retention and minimized washout. Innovatively, this study proposes a carrier-granular sludg synergistic
465 microenvironment strategy, elucidates how carrier type and introduction timing regulate biofilm
466 functionality, and provides both theoretical insights and practical guidance for optimizing CANON
467 process applications.

468 **Author contributions** Jun-hao Jiang: Data curation, Methodology, Writing-Original draft. Shi-han
469 Zhu: Data curation, Investigation. Fu-hao Li: Data curation, Investigation. Hai-xia He: Data curation,
470 Investigation. Xiao Fang: Data curation, Investigation. Ya-lei Liu: Data curation, Investigation,
471 Visualization. Li-juan Feng: Writing-review & editing, Resources. Guang-feng Yang: Methodology,
472 Investigation, Writing-review & editing, Resources.

473 **Funding** This research was supported by Zhejiang Provincial Natural Science Foundation of China
474 under Grant No. LY23E080006 and National Natural Science Foundation of China under Grant No.
475 51808498.

476 **Competing interests** The authors declare that they have no known competing financial interests or
477 personal relationships that could have appeared to influence the work reported in this paper.

478 **Ethical approval** This article does not contain any studies with human participants or animals
479 performed by any of the authors.

480 **Data Availability Statement** The data that support the findings of this study are available from the
481 corresponding author upon reasonable request.

482 **References**

483 Adams M, Xie JX, Xie JW, Chang YF, Guo ML, Chen CJ, Zhang TC (2020) The effect of carrier
484 addition on Anammox start-up and microbial community: a review. Rev Environ Sci Bio 19:
485 355-368.
486 Ahmad HA, Ni SQ, Ahmad S, Zhang J, Liang JL, Yang GF (2020) Gel immobilization: A strategy to
487 improve the performance of anaerobic ammonium oxidation (anammox) bacteria for nitrogen-rich
488 wastewater treatment. Bioresour Technol 313: 123642.
489 Aktan CK, Yapsakli K, Mertoglu B (2012) Inhibitory effects of free ammonia on Anammox bacteria.
490 Biodegradation 23: 751-762.
491 Anthonisen A, Loehr R, Prakasam T, Srinath E (1976) Inhibition of nitrification by ammonia and
492 nitrous acid. Water Pollut 48(5): 835-852.
493 Aqeel H, Asefa B and Liss SN (2023) Nitrospira dominant pin-point flocs with granule-like
494 settleability in stirred tank reactors with oxic/hypoxic/oxic zones. Front Microbiol 14:1307727.
495 Castro-Barros CM, Daelman MRJ, Mampaey KE, van Loosdrecht MCM, Volcke EIP (2015) Effect of
496 aeration regime on N2O emission from partial nitritation-anammox in a full-scale granular sludge
497 reactor. Water Res 68: 793-803.
498 Chang BZ, Huang XL, Chen DZ, Jin RC, Feng LJ, Yang GF (2025b) How biofilm and granular sludge
499 cope with dissolved oxygen exposure in anammox process: Performance, bioaccumulation
500 characteristics and bacterial evolution. J Environ Manage 373: 123986.
501 Chang BZ, Zhao YC, Zhang S, Luo Q, Chen DZ, Jin RC, Feng LJ, Yang GF (2025a) Adaptive changes
502 of biofilm and sludge in CANON process under various organics stresses: Performance, biomass
503 characteristics and metabolic pathways. Process Saf Environ Prot 197: 107091.

504 Chen CJ, Jiang Y, Zou XY, Guo ML, Liu H, Cui MH, Zhang TC (2021) Insight into the influence of
505 particle sizes on characteristics and microbial community in the anammox granular sludge. J Water
506 Process Eng 39: 101883.
507 Chen JW, Zheng P, Yu Y, Mahmood Q, Tang CJ (2010) Enrichment of high activity nitrifiers to
508 enhance partial nitrification process. Bioresour Technol 101(19): 7293-7298.
509 Chen YP, Li C, Guo JS, Fang F, Gao X, Zhang P, Li S (2013) Extraction and Characterization of
510 Extracellular Polymeric Substances in Biofilm and Sludge via Completely Autotrophic Nitrogen
511 Removal Over Nitrite System. Appl Biochem Biotechnol 169: 526-538.
512 Feng CJ, Lotti T, Lin Y, Malpei F (2019) Extracellular polymeric substances extraction and recovery
513 from anammox granules: Evaluation of methods and protocol development. Chem Eng J 374:
514 112-122.
515 Froelund B, Griebe T, Nielsen PH (1995) Enzymatic activity in the activated-sludge floc matrix. Appl
516 Microbiol Biot 43: 755-761.
517 Fu KM, Li ZR, Wang HF, Zhang XJ, Ma BB, Yang GF (2025) Effects of aeration conditions on
518 nitrogen removal performance and N_2O emissions in a biofilm CANON reactor. Biochem Eng J 219:
519 109724.
520 Fukami T (2015) Historical contingency in community assembly: integrating niches, species pools, and
521 priority effects. Annu Rev Ecol Evol Syst 46: 1-23.
522 García-Ruiz MJ, Mazamárquez P, González-López J, Osorio F (2018) Nitrogen removal capacity and
523 bacterial community dynamics of a canon biofilter system at different organic matter concentrations.
524 Chemosphere 193: 591-601.

525 Gilbert EM, Agrawal S, Karst SM, Horn H, Nielsen PH, Lackner S (2013) Low temperature partial
526 nitritation/anammox in a moving bed biofilm reactor treating low strength wastewater. Environ Sci
527 Technol 48(15): 8784-8792.
528 Gong XF, Wang B, Qiao X, Gong QT, Liu XF, Peng YZ (2020) Performance of the anammox process
529 treating low-strength municipal wastewater under low temperatures: effect of undulating seasonal
530 temperature variation. Bioresour Technol 312: 123590.
531 He ST, Niu QG, Ma HY (2015) The Treatment Performance and the Bacteria Preservation of
532 Anammox: A Review. Water Air Soil Pollut 226: 163.
533 Hu MN, Liu XJ, Ya T, Liu JY, Zhang ML, Wang XH (2023) Dissolved oxygen alters the microbial
534 interactions of anammox consortia in PN/A process. J Water Process Eng 53: 103697.
535 Jin RC, Yang GF, Yu JJ, Zheng P (2012) The inhibition of the Anammox process: A review. Chem Eng
536 J 197: 67-79.
537 Keren R, Lawrence JE, Zhuang WQ, David J, Banfield JF, Cohen LA, Zhou LJ, Yu K (2020) Increased
538 replication of dissimilatory nitrate-reducing bacteria leads to decreased anammox bioreactor
539 performance. Microbiome 8: 7.
540 Kindaichi T, Yuri S, Ozaki N, Ohashi A (2012) Ecophysiological role and function of uncultured
541 Chloroflexi in an anammox reactor. Water Sci Technol 66(12): 2556-2561.
542 Kouba V, Svehla P, Catrysse M, Prochazkova L, Radechovska H, Jenicek P, Bartacek J (2019) How
543 biomass growth mode affects ammonium oxidation start-up and NOB inhibition in the partial
544 nitritation of cold and diluted reject water. Environ Technol 40(6): 673-682.

545 Kraiem K, Kallali H, Wahab MA, Fra-vazquez A, Mosquera-Corral A, Jedidi N (2019) Comparative
546 study on pilots between ANAMMOX favored conditions in a partially saturated vertical flow
547 constructed wetland and a hybrid system for rural wastewater treatment. Sci Total Environ 670:
548 644-653.
549 Kuypers MMM, Marchant HK, Kartal B (2018) The microbial nitrogen-cycling network. Nat Rev
550 Microbiol 16: 263-276.
551 Li J, Wang D, Yu DS, Zhang PY (2018) Performance and sludge characteristics of anammox process at
552 moderate and low temperatures. Korean J Chem Eng 35: 164-171.
553 Liu T, Li D, Zhang J, Lv Y, Quan X (2016) Effect of temperature on functional bacterial abundance and
554 community structure in CANON process. Biochem Eng J 105: 306-313.
555 Liu YW, Sun J, Peng L, Wang DB, Dai XH, Ni BJ (2016) Assessment of Heterotrophic Growth
556 Supported by Soluble Microbial Products in Anammox Biofilm using Multidimensional Modeling.
557 Sci Rep 6: 27576.
558 Loewus FA (1952) Improvement in anthrone method for determination of carbohydrates. Anal Chem
559 24: 219.
560 Lotti T, Carretti E, Berti D, Martina MR, Lubello C, Malpei F (2019) Extraction, recovery and
561 characterization of structural extracellular polymeric substances from anammox granular sludge. J
562 Environ Manage 236: 649-656.
563 Luo JJ, Wu YC, Fu HY, Wang J, Li J, Wang DB (2024) Shift in microorganism and functional gene
564 abundance during completely autotrophic nitrogen removal over nitrite (CANON) process. J Environ
565 Manage 359: 121009.

566 Lv YF, Pan JJ, Huo TR, Li D, Zhang XJ, Yang GF (2019) Enhanced microbial metabolism in one stage
567 partial nitritation-anammox system treating low strength wastewater by novel composite carrier.
568 Water Res 163: 114872.
569 Mulder A, van de Graaf AA, Robertson LA, Kuenen JG (1995) Anaerobic ammonium oxidation
570 discovered in a denitrifying fluidized bed reactor. FEMS Microbiol Ecol 16(3): 177-184.
571 Nielsen M, Bollmann A, Sliekers O, Jetten M, Schmid M, Strous M, Schmidt I, Larsen LH, Nielsen LP,
572 Revsbech NP (2005) Kinetics, diffusional limitation and microscale distribution of chemistry and
573 organisms in a CANON reactor. FEMS Microbiol Ecol 51(2): 247-256.
574 Nobuyuki Y, Ryota M, Hideyuki Y, Tatsuaki H, Hisayoshi I, Takayuki A, Masaaki H, Akihiko T (2019)
575 Startup, performance, and microbial communities of an anammox reactor inoculated with indigenous
576 sludge for the treatment of high-salinity and mesophilic underground brine. Clean Technol Environ
577 Policy 21: 1001-1011.
578 Pereira AD, Cabezas A, Etchebehere C, Chernicharo CAL, Araujo JC (2017) Microbial communities in
579 anammox reactors: a review. Environ Technol Rev 6: 74-93.
580 Pynaert K, Smets BF, Beheydt D, Verstraete W (2004) Start-up of autotrophic nitrogen removal
581 reactors via sequential biocatalyst addition. Environ Sci Technol 38: 1228-1235.
582 Schneier A, Melaugh G, Sadler JC (2024) Engineered plastic-associated bacteria for biodegradation
583 and bioremediation. Biotechnol Environ 1:7.
584 Sheng GP, Yu HQ, Li XY (2010) Extracellular polymeric substances (EPS) of microbial aggregates in
585 biological wastewater treatment systems: A review. Biotechnol Adv 28: 882-894

586 Sura A, Stavropoulos A, Jenkins B, Graves S, Ahmadi A, Marzbanrad V, Che G, Cheng J, Tan H, Wei
587 X, Egan S, Ingalls B, Neufeld JD, Ulrich E, Charles TC, Doxey AC (2025) Comparative proteomics
588 of biofilm development in Pseudoalteromonas tunicata discovers a distinct family of
589 Ca2+-dependent adhesins. mBio 16(6): e01069-25.
590 Tang CJ, Zheng P, Mahmood Q, Chen JW (2010) Effect of substrate concentration on stability of
591 anammox biofilm reactors. J Cent South Univ Technol 17: 79-84.
592 Tang CJ, Zheng P, Wang CH, Mahmood Q, Zhang JQ, Chen XG, Zhang L, Chen JW (2011)
593 Performance of high-loaded ANAMMOX UASB reactors containing granular sludge. Water Res 45:
594 135-144.
595 Wang L, Zheng P, Xing YJ, Li W, Yang J, Abbas G, Liu S, He ZF, Zhang JQ, Zhang HT, Lu HF (2014)
596 Effect of particle size on the performance of autotrophic nitrogen removal in the granular sludge bed
597 reactor and microbiological mechanisms. Bioresour Technol 157: 240-246.
598 Wang WG, Wang H, Jiang ZW, Wang YY (2020) Visual evidence for anammox granules expanding
599 their size by aggregation of anammox micro-granules. Sci Total Environ 745: 141052.
600 Wang WG, Wang YY, Wang XD, Zhang Y, Yan Y (2019) Dissolved oxygen microelectrode
601 measurements to develop a more sophisticated intermittent aeration regime control strategy for
602 biofilm-based CANON systems. Chem Eng J 365: 165-174.
603 Wang WG, Yan Y, Song CK, Pan ML, Wang YY (2018) The microbial community structure change of
604 an anaerobic ammonia oxidation reactor in response to decreasing temperatures. Environ Sci Pollut
605 Res 25: 35330-35341.

606 Wang XT, Yang H, Liu XY, Li D, Zhang XJ, Yang GF (2022) Formation mechanisms and assembly
607 patterns of anammox biofilm induced by carrier type: Novel insights based on low-strength
608 wastewater treatment. Bioresour Technol 362: 127863.
609 Xia QQ, Shang W, Zheng XC, Zhang WA, Wang YX, Sun YL, Li PF (2024) Effect of aeration on
610 low-substrate CANON process. Water Sci Eng 17: 292-299.
611 Xu HH, Wang XJ, Wang MY, Li D, Zhang XJ, Yang GF (2025) Metatranscriptomics provides an
612 in-depth perspective on the resistance and detoxification of anammox bacteria to dissolved oxygen
613 in a pilot CANON process. Water Res 268: 122613.
614 Xu HH, Wang XJ, Wang MY, Wu JB, Zhang B, Wang JS, Zhang QT, Lin BR, Chen SH (2025)
615 Metatranscriptomics provides an in-depth perspective on the resistance and detoxification of
616 anammox bacteria to dissolved oxygen in a pilot CANON process. Water Res 268: 122613.

617 Ye YY, Ngo HH, Guo WS, Chang SW, Nguyen DD, Varjani S, Liu Q, Bui XT, Hoang NB (2022)
618 Bio-membrane integrated systems for nitrogen recovery from wastewater in circular bioeconomy.
619 Chemosphere 289: 133175.
620 Yu CZ, Zhang XY, Zhao SH, Wang DB, Li XY, Yang GF (2021) Sludge granulation and microbial
621 activity in a stable CANON process by DO controlling and operating parameter optimization.
622 Biochem Eng J 174: 108126.
623 Yue X, Yu GP, Lu YQ, Liu ZH, Li QH, Tang JL, Liu J (2018) Effect of dissolved oxygen on nitrogen
624 removal and the microbial community of the completely autotrophic nitrogen removal over nitrite
625 process in a submerged aerated biological filter. Bioresour Technol 254: 67-74.
626 Zhang L, Wang YP, Soda S, Ike M, Yang GF (2020) Effect of fulvic acid on bioreactor performance
627 and on microbial populations within the anammox process. Bioresour Technol 318: 124094.
628 Zhang S, Lai LY, Wang TX, Jin WL, Yi RR, Chen DZ, Jin RC, Yang GF (2024) Response of anammox
629 to organics with different degradation characteristics and exposure time: Performance, sludge
630 characteristics and bacterial community. Sci Total Environ 951: 175650.
631 Zhao YP, Liu SF, Jiang B, Feng Y, Zhu TT, Tao HC, Tang X, Liu S (2018) Genome-Centered
632 Metagenomics Analysis Reveals the Symbiotic Organisms Possessing Ability to Cross-Feed with
633 Anammox Bacteria in Anammox Consortia. Environ Sci Technol 52(19): 11285-11296.
634 Zhou Z, Ming Q, An Y, Ruan DN, Chen G, Wei HJ, Wang MY, Wu ZC (2021) Performance and
635 microbial community analysis of anaerobic sludge digestion enhanced by in-situ microaeration. J
636 Water Process Eng 42: 102171.

637 Zhu TT, Lai WX, Zhang YB, Liu YW (2022) Feammox process driven anaerobic ammonium removal
638 of wastewater treatment under supplementing Fe(III) compounds. Sci Total Environ 804: 149965.
639

640 **Figure captions**

641 **Fig. 1 Reactor diagram**

642 **Fig. 2 Operation performance of reactor at each stage: (a) NH_4^+-N, NO_2^--N and TN concentration,**

643 **(b) NH_4^+-N and TN removal efficiency with TN rate**

644 **Fig. 3 Operation performance of reactors R1 and R2: (a) R1 and (b) R2**

645 **Fig. 4 TB-EPS content of sludge with different particle sizes**

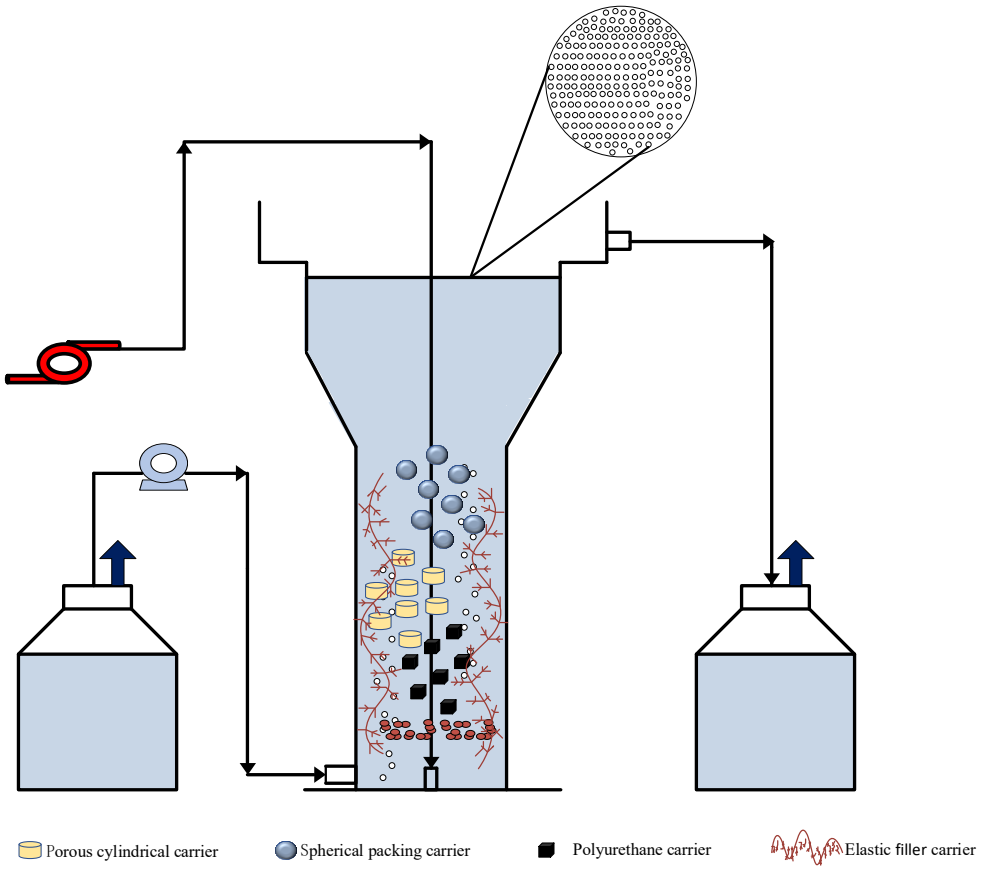
646 **Fig. 5 3D-EEM of EPS in sludge with different particle sizes**

647 **Fig. 6 Bacterial structure of biofilm and sludge samples: (a) biofilm and sludge at phylum level,**

648 **(b) genus level of each sludge sample with different particle sizes and (c) genus level of biofilm**

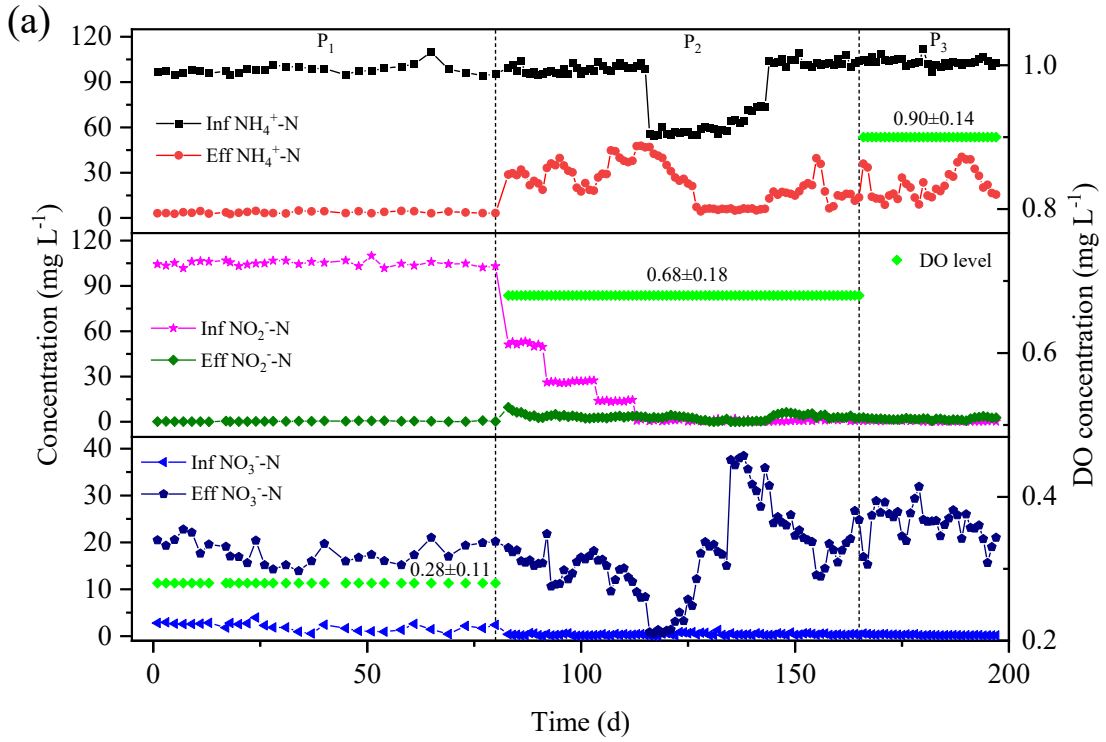
649 **Fig. 7 Nitrogen removal related functional gene composition of sludge (a) and biofilm (b) samples**

650 **Figure 1**

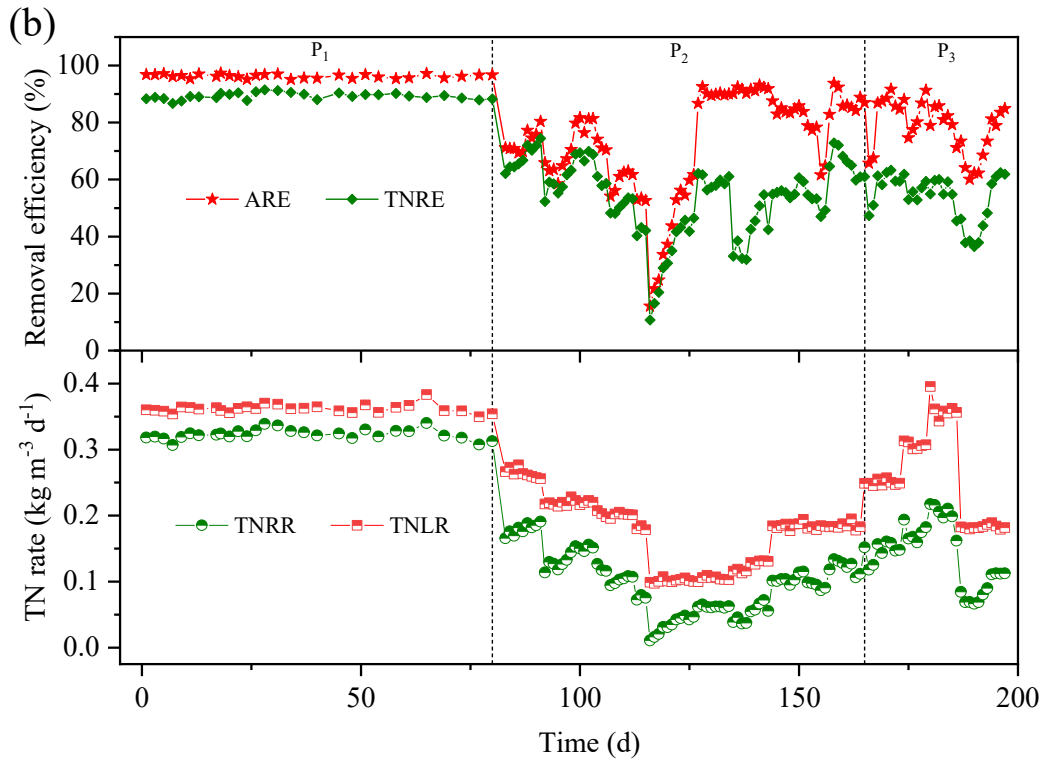


651

652 **Figure 2**

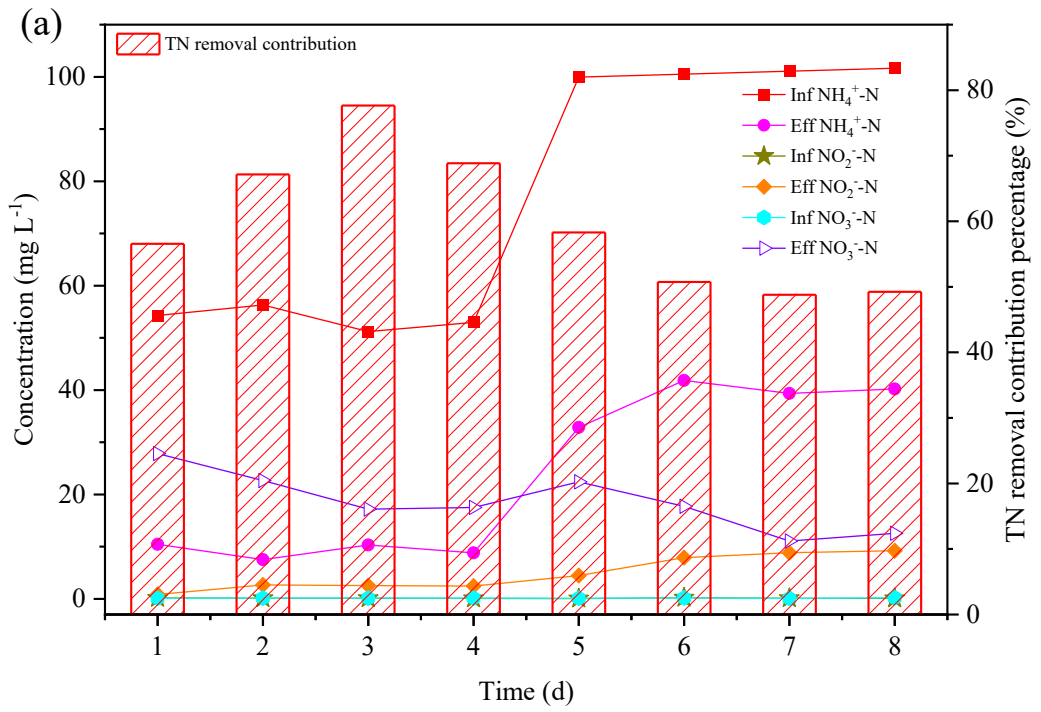


653

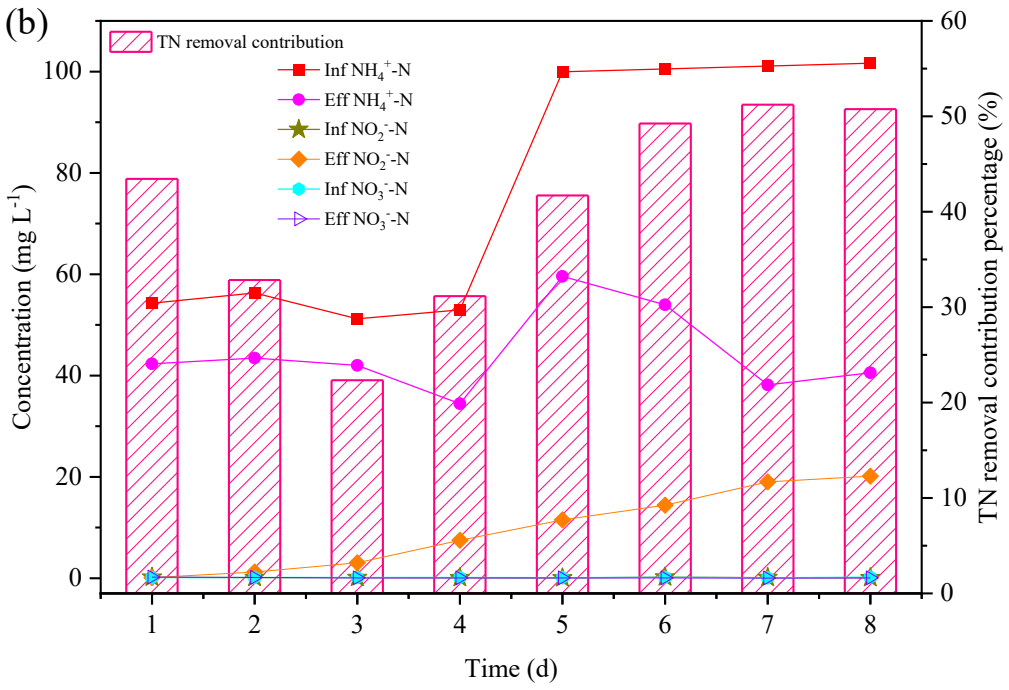


654

655 **Figure 3**

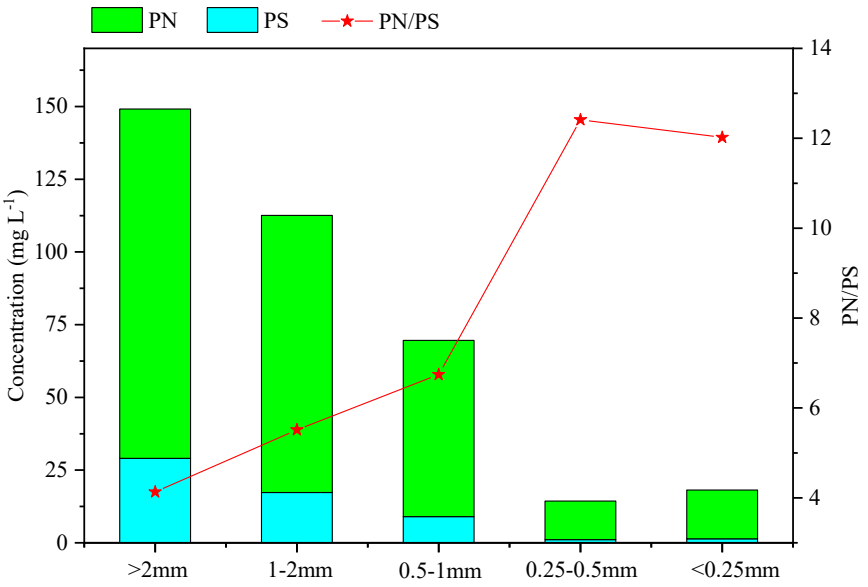


656



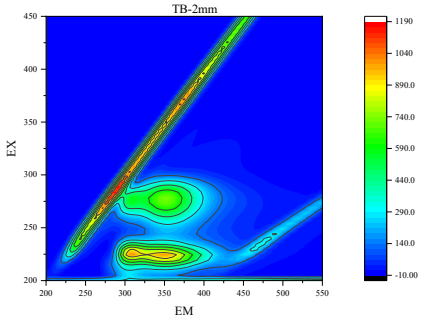
657

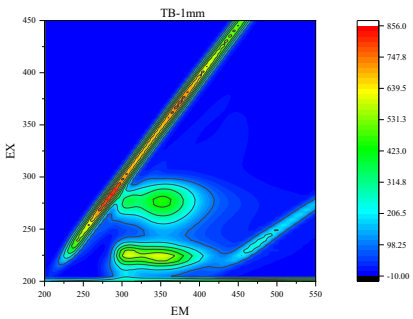
658 **Figure 4**



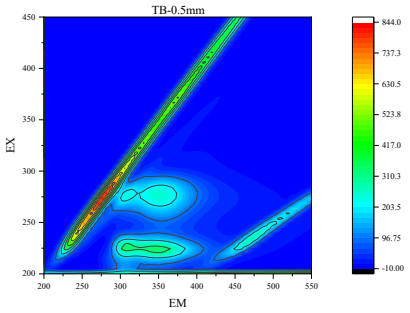
659

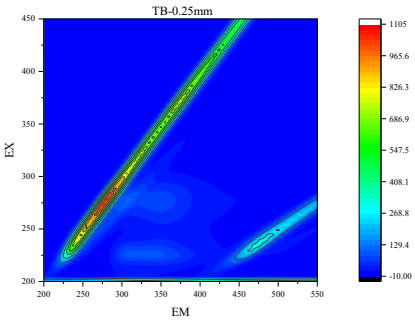
660 **Figure 5**



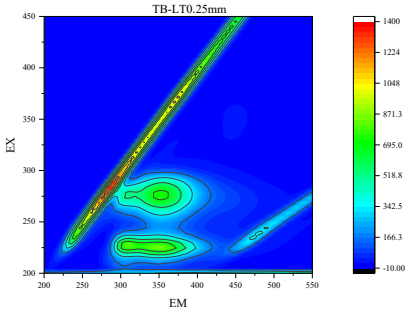


661





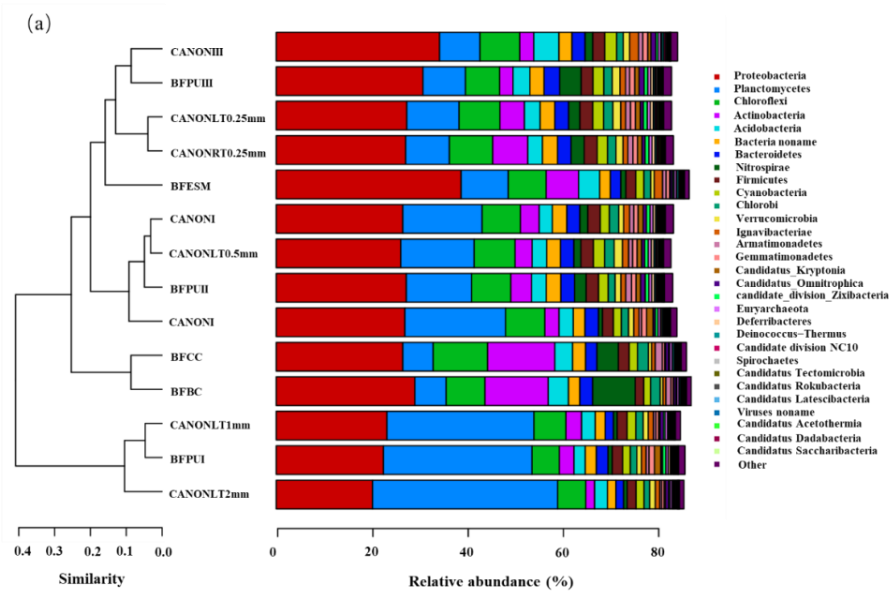
662



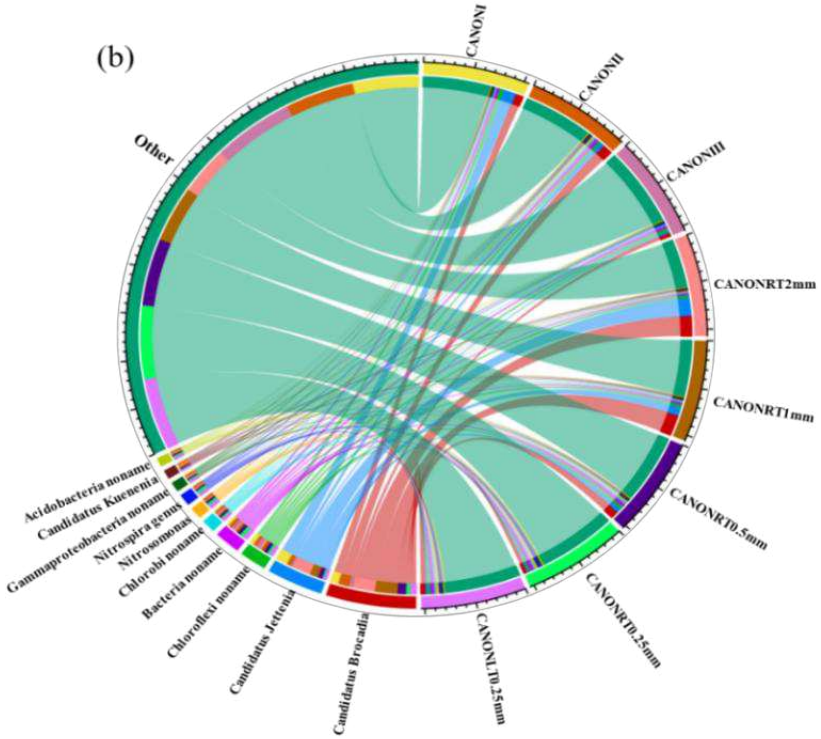
663

664

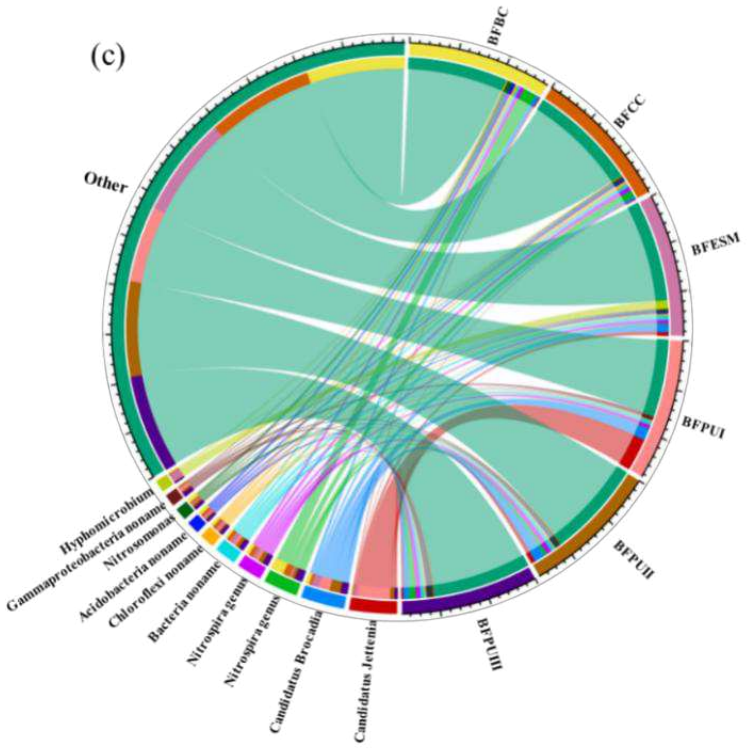
665 **Figure 6**



666



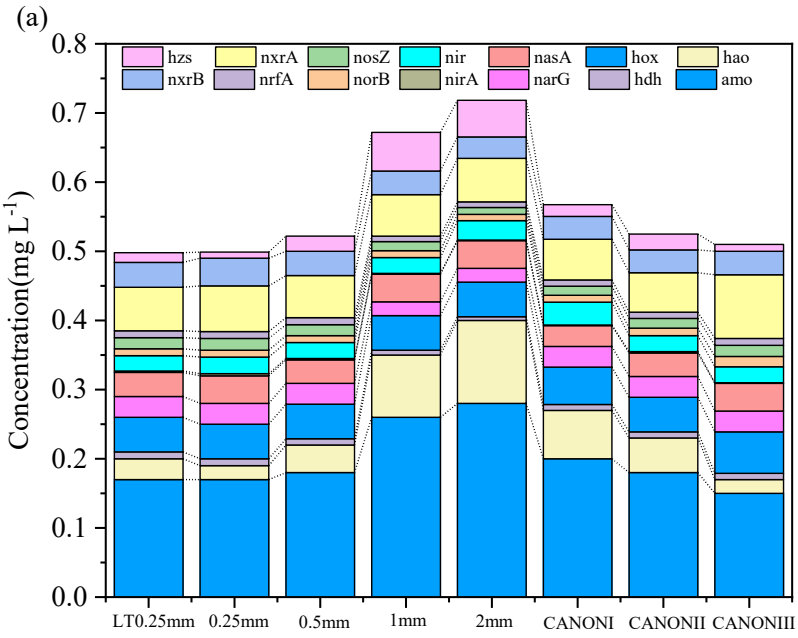
667


(c)
BFBC
BFCC
BFESM
BFPUI
BFPUII
BFPUIII
Candidatus Jettenia
Candidatus Brocadia
Nitrospira genus
Nitrospira genus
Bacteria noname
Chloroflexi noname
Acidobacteria noname
Nitrosomonas
Gammaproteobacteria noname
Hyphomicrobium
Other

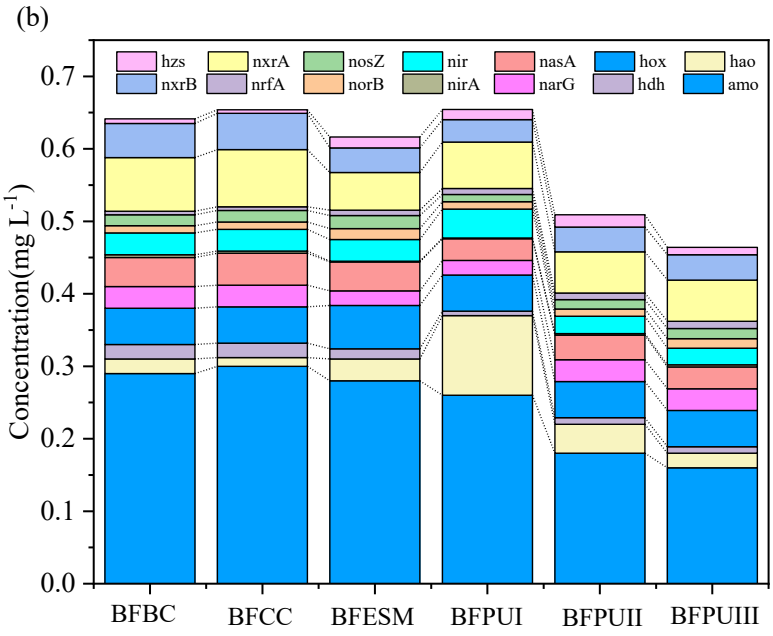
668

669

670 **Figure 7**



671



672

673

674 **Tables**

675 **Table 1 Main operation parameters of reactor at each stage**

Phase	Operation period (d)	HRT (h)	DO (mg L^{-1})	Influent (mg L^{-1})		NLR (kg m^{-3} d^{-1})	NRR (kg m^{-3} d^{-1})
				NH_4^+-N	NO_2^--N		
P1	1-80	14.4	0.28±0.11	98.1±3.00	104.9±1.80	0.36±0.006	0.32±0.008
P2	81-165	14.4	0.68±0.18	87.1±19.43	11.5±16.80	0.18±0.05	0.10±0.05
P3	166-197	7.2-14.4	0.90±0.14	103.4±2.73	0.5±0.41	0.26±0.07	0.14±0.05

676

677 **Table 2 Sludge loss of CANON reactor**

Characteristic	1d	2d	3d	4d	5d	6d	7d	8d
SS(g)	21.3	7.9	6.1	11.9	4.7	1.5	0	0
VSS(g)	8.3	5.8	2.2	5.0	0.7	1.0	0	0
VSS/SS(%)	39.0	73.4	36.1	42.0	14.9	66.7	0	0

678

679 **Table 3 Bacterial diversity of carrier biofilm and sludge samples**

Sample	Gene	Shannon	Simpson
BFBC	1385666	12.91	6.0e-06
BFCC	1460377	13.00	6.0e-06
BFESM	1392386	12.53	1.3e-05
BFPUI	1465465	11.93	5.7e-05
BFPUII	1699206	12.93	1.1e-05
BFPUIII	1836440	13.07	8.0e-06
CANONI	1606492	12.53	2.2e-05
CANONII	1810514	12.82	1.5e-05
CANONIII	1406495	12.50	1.2e-05
CANON2mm	1655963	13.08	7.0e-06
CANON1mm	1730125	12.92	1.1e-05
CANON0.5mm	1274406	11.94	4.5e-05
CANON0.25mm	1219582	11.60	6.5e-05
CANONLT0.25mm	1633342	13.07	8.0e-06

680 Note: I, II, and III represent stages P1, P2, and P3, respectively; BFBC represents spherical packing,

681 BFCC represents cylindrical packing, BFESM represents elastic packing, BFPU represents

682 polyurethane packing, and CANON represents CANON sludge.